

## INTRODUCTION

In the last decade, the oxygen A-band, centered on 760 nm, has been the subject of several spectroscopic investigations as summarized recently by *Brown and Plymate* [2000]. This band will be used in the SAGE III experiment to provide altitude registration, and it is therefore crucial to have the most accurate possible line parameter information on it. To this end, *Brown and Plymate* [2000] conducted a very careful laboratory study of line intensities and broadening coefficients of the A band, which resulted in an improved set of line parameters.

In satellite experiments measuring atmospheric transmission of solar radiation, one typically encounters extremely long optical paths containing as many as 30 air masses. (One air mass is the number of molecules in an optical path from the surface to the top of the atmosphere when looking straight up.) Such long paths cannot be achieved under laboratory conditions. However, a high altitude balloon experiment, viewing the sun in occultation mode, achieves similar path lengths.

The present study investigated absorption by the A band under such long path conditions from a balloon platform using a Fourier Transform Spectrometer (FTS). We were able to track the sun to zenith angles greater than  $95^\circ$  and tangent altitudes below 10 km, viewing through  $\sim 30$  air masses. A secondary goal of the experiment was to measure the water vapor spectrum in the 940 nm region, and the instrument was equipped with a second channel for this purpose. Unfortunately, this channel did not perform well during the flight, and no useable data were obtained.

## INSTRUMENTATION

The interferometer used for this experiment was a BOMEM DA2 Michelson interferometer-spectrometer with two inch input optics and a maximum achievable optical path difference of 50 cm. For this flight, the instrument was set to 20 cm maximum path difference, resulting in an unapodized FWHM resolution of  $0.025 \text{ cm}^{-1}$ . This choice was chosen to minimize the scan time, thus reducing the effects of "interferogram smearing" (changing optical path during the scan); also because the Doppler width of  $\text{O}_2$  at 760 nm is  $\sim 0.025 \text{ cm}^{-1}$ , recording spectra at higher resolution would not have substantially increased the observed resolution. The scan time was  $\sim 24$  seconds, and data were recorded in both the forward (Zero Path Difference (ZPD) at the beginning of the scan) and reverse (ZPD at the end of scan) directions. The instrument was equipped with a quartz beam splitter and had a field of view (FOV) of  $\sim 0.1^\circ$ . Optical alignment was maintained during each scan using the BOMEM dynamic alignment system, in which a dual axis servo system maintains the phase relationship on a set of photo diodes illuminated by the sampling laser by making small adjustments of the instrument's fixed mirror. The output beam from the interferometer was divided by a mirror positioned to reflect half of the beam onto the short wavelength (760 nm) detector and pass the other half to the long wavelength (940 nm) detector. Both detectors were photo-diodes. The sampling interval, digital and optical filters were selected so that the bandpasses measured were  $12839.0\text{-}13333.6 \text{ cm}^{-1}$  (779 - 750 nm) and  $10370.6\text{-}10864.4 \text{ cm}^{-1}$  (964 - 920 nm).

Gross azimuthal alignment ( $\pm \sim 5^\circ$ ) of the instrument was achieved with a rotator motor from which the payload was suspended. The rotator was controlled by the feedback from a pair of calibrated

magnetometers mounted on the gondola. The rotator could either maintain a preset angle, or be turned via telemetry command from the ground. The input solar beam was maintained on the interferometer input aperture using a biaxial solar tracking telescope designed and constructed at DU. The interferograms and various house keeping data were recorded onboard using a custom personal computer writing to a solid state hard drive. The spectrometer and ancillary hardware were controlled from the ground via a series of telecommands sent from the command center allowing cycling of the computer, the spectrometer, spectrometer heaters, the solar tracker, and the rotator.

## **FLIGHT DETAILS**

The payload was launched at 1705 CDT on 7 July, 2000, from the National Scientific Balloon Facility (NSBF) site in Palestine, Texas. The balloon reached a float altitude of 33 km at 19:30, approximately 33 minutes before the beginning of sunset (solar zenith angle =  $90^\circ$ ). Data were recorded during the balloon ascent and during the occultation period until loss of signal occurred at 2106 CDT at which time the solar zenith angle at the balloon location was  $> 95.69^\circ$ , corresponding to a tangent height for a ray from the sun to the payload of 6.3 km. The location and altitude of the payload was determined from GPS data provided by NSBF. The NSBF package on the payload was equipped with a transponder, as required by the Federal Aviation Administration as a safety precaution for commercial airliner safety. This device is typically in operation at altitudes below 70,000 feet, and sometimes interferes with the instrument data stream. This appears to have been the case during this flight; the data recorded during the first part of the balloon ascent is quite noisy.

## **DATA REDUCTION and ANALYSIS**

The interferograms were processed after the flight on a DEC-Alpha computer. The interferograms were phase corrected using the convolution technique [Foreman, *et al.* 1966] and then added in reverse-forward pairs to further mitigate the effects of smearing. For solar zenith angles less than  $93.5^\circ$ , the scans were generally added in fours to increase the signal to noise ratio. Figure 1 shows the tangent height and air mass as a function of solar zenith angle for the flight.

In order to generate transmission spectra from the transformed data, an envelope representing the combined effects of the digital and optical filter and the detector response was generated from a set of twenty averaged "high sun" (i.e., pre-sunset) scans. This was done by selecting points between the oxygen lines, and fitting a cubic spline to them. Figure 2 shows the averaged high sun spectrum and resulting envelope. Figure 3 shows a series of occultation scans which have been divided by this envelope. These spectra have not been vertically shifted; the offset between successive scans is due to the strong continuum contribution to the long path absorption.

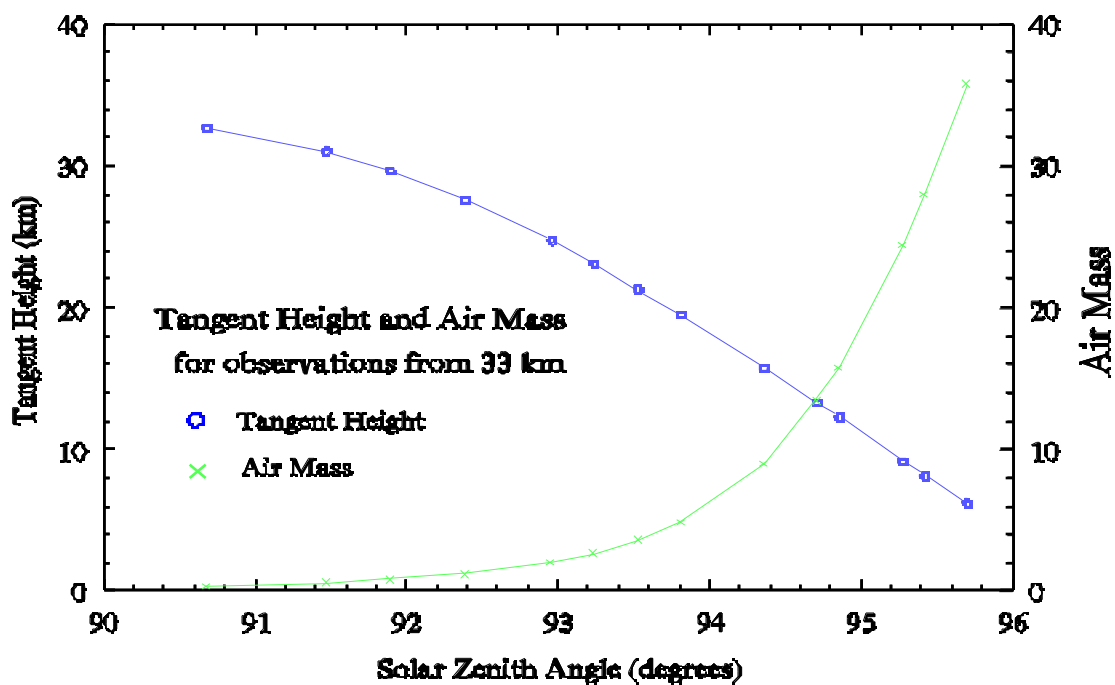


Figure 1. Air mass and tangent height as functions of solar zenith angle for a balloon at 33 km.

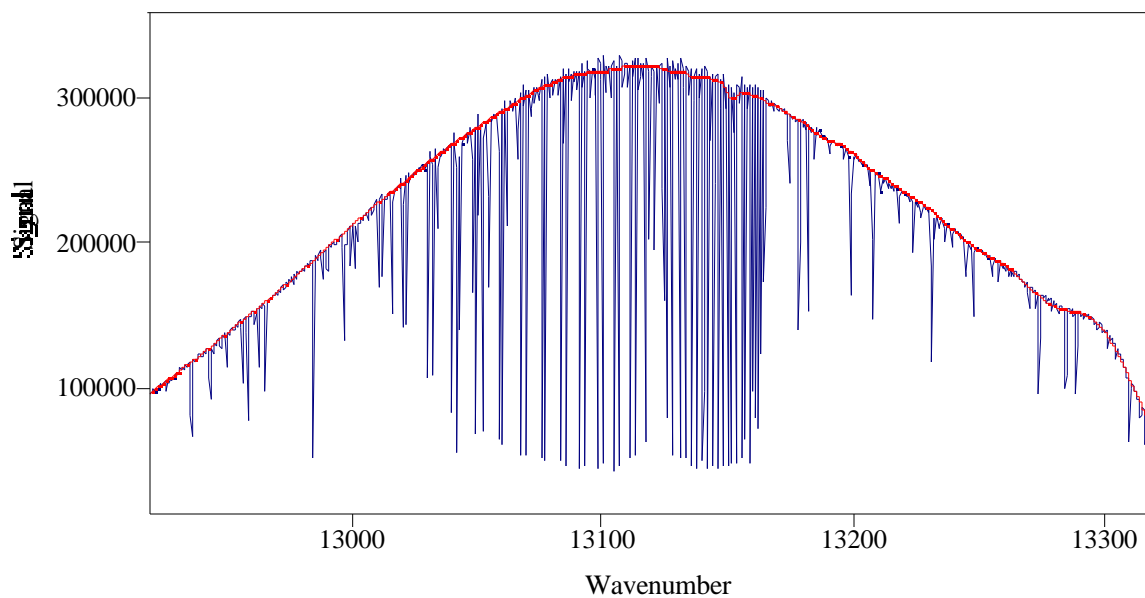


Figure 2. Averaged high sun spectrum and the background envelope generated from it.

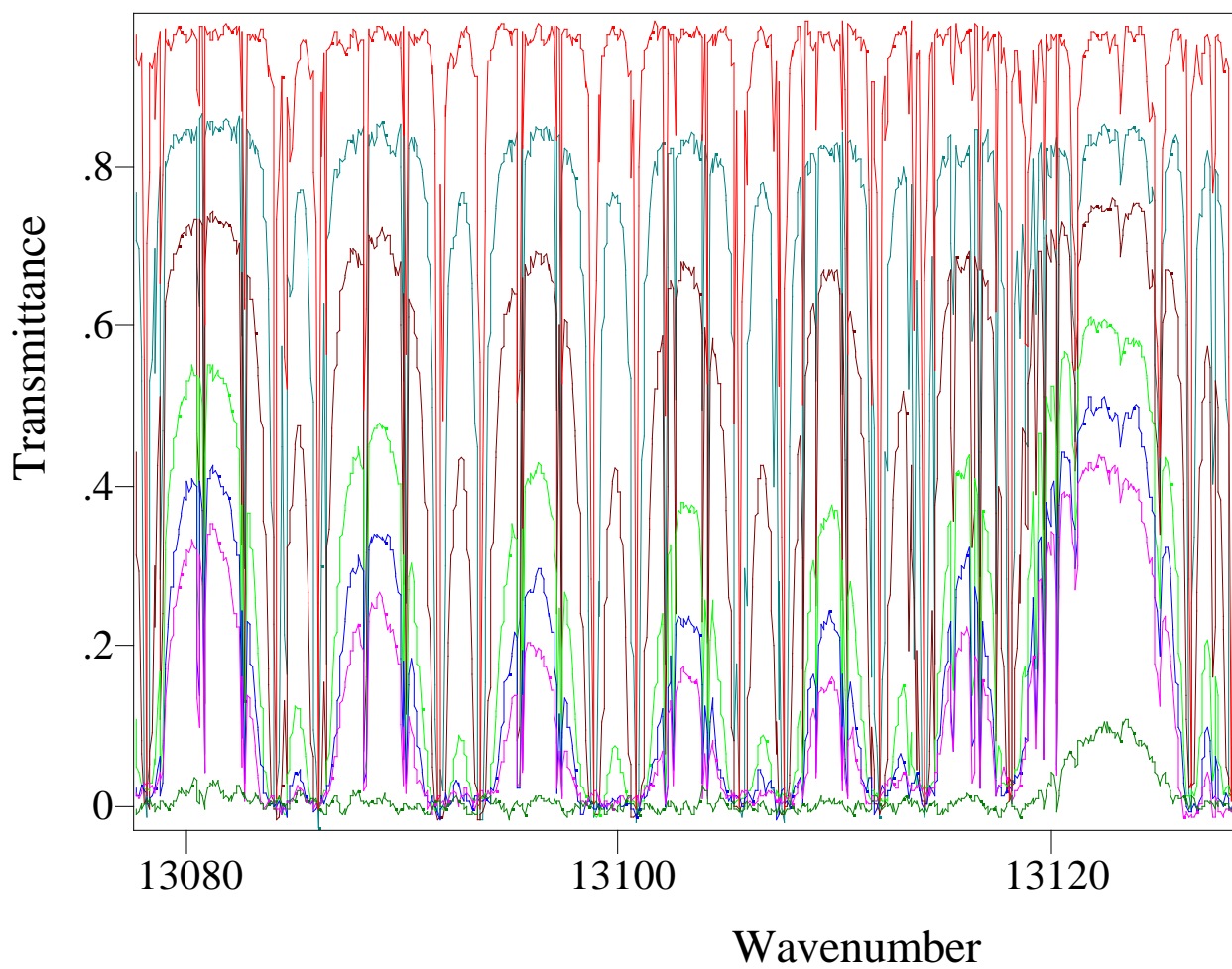


Figure 3. Sequence of sunset scans at solar zenith angles of  $91.24^\circ$ ,  $92.94.57^\circ$ ,  $94.70^\circ$ , and  $95.41^\circ$

## RESULTS

### Comparison to Synthetic Spectra

Synthetic spectra were generated using the radiative transfer code LBLRTM (Line-By-Line Radiative Transfer Model) [Clough, 1992]. A pressure, temperature profile generated from radiosonde data from Brownsville, Dallas, and Shreveport combined with data provided by NSBF from on-board sensors, was used as input for the calculations. Figure 4 shows this profile. HITRAN92 line parameters with the modifications of Brown and Plymate [2000] were used in the calculations.

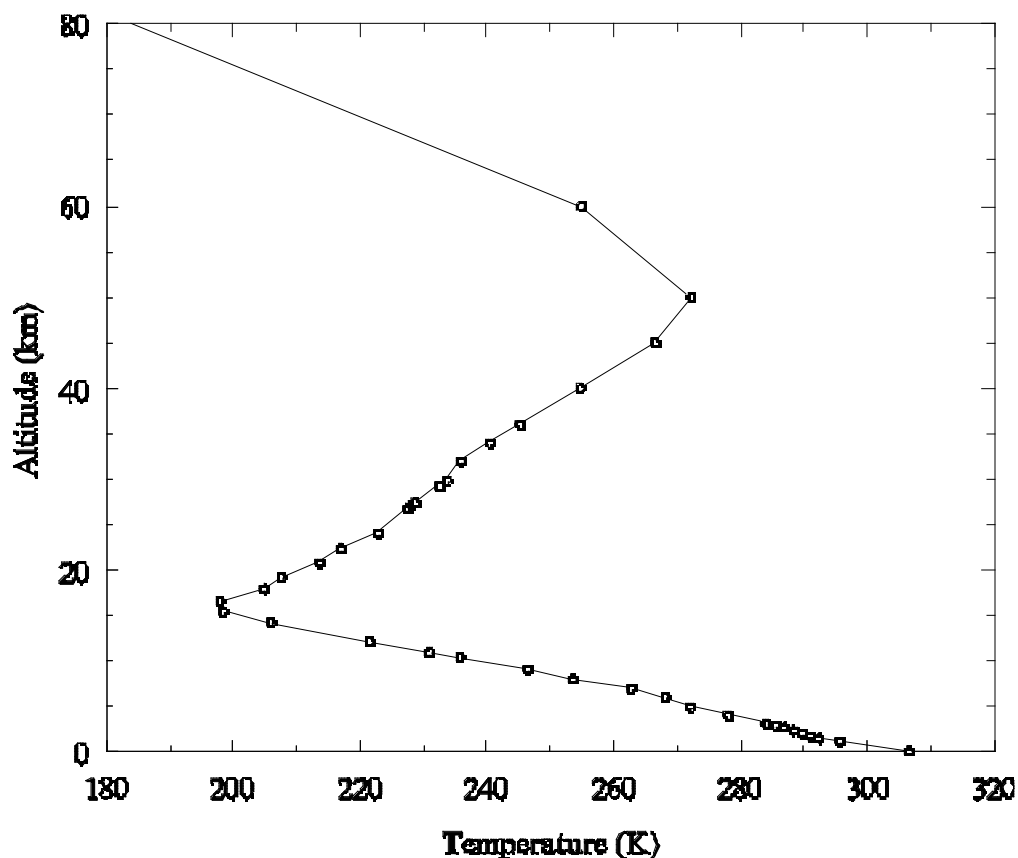


Figure 4. Temperature profile used in generating synthetic spectra. Sonde and flight data were smoothly joined to a standard midlatitude atmosphere above the balloon altitude.

Figure 5 shows a comparison between observed and calculated spectra for the averaged high sun spectrum used to generate the envelope. The series of lines near  $13122\text{ cm}^{-1}$  (and elsewhere) not appearing in the synthetic spectrum are solar lines, arising from absorption in the sun's atmosphere, which are not included in the calculation. Kurucz [1992] has generated a database of solar lines, and Figures 6&7 show a comparison between those lines and the current data. One sees that in general,

the agreement is good, but there are several discrepancies. Lines predicted near  $13110\text{ cm}^{-1}$  do not appear in the data, whereas lines near  $12958\text{ cm}^{-1}$  are either missing in the compilation or are significantly weaker than observed.

As indicated above, data obtained during the first part of the balloon ascent was very noisy and essentially unusable, presumably because of transponder interference. Data recorded during the later part of the ascent do not have this difficulty, and Figure 8 shows a comparison between computed and observed spectra for an altitude of 18.46 km and a zenith angle of  $68.81^\circ$ .

Figure 9 illustrates a problem with incorrect line positions of  $^{16}\text{O}^{18}\text{O}$  isotopic lines, which become increasingly displaced away from the band center, while Figure 10 shows the complete absence of the  $^{16}\text{O}^{17}\text{O}$  lines from HITRAN96.

### **Continuum Absorption**

As mentioned above, and displayed in Figure 3, the A band line absorption is superimposed on a strong continuum absorption. The laboratory measurements of Brown and Plymate [2000] (and other investigators) show no evidence of an  $\text{O}_2$  continuum, present in other  $\text{O}_2$  bands (e.g., the 1.27 micron region), in the A band region. The observed continuum in the A band region appears to be attributable to a combination of continua effects arising from the  $\text{O}_3$  Chappuis band, Rayleigh scattering, and aerosol scattering. These effects are illustrated in Figure 11, which shows the individual continua and their combined effect in the A band region. One sees that for a zenith angle of  $94.85^\circ$ , the combined modeled continuum absorption is  $\sim 56\%$ , and in fact is larger than the observed continuum away from the band center by about 15%, as shown in the figure. The aerosol model selected for this calculation is the LBLRTM "background stratosphere" model. Since user control over the aerosol model in LBLRTM is limited, and since the Rayleigh and aerosol continua are essentially parallel over the A band region (Figure 11), in subsequent calculations the aerosol model was deselected and the Rayleigh contribution was multiplied by a factor of  $\sim 1.3$  to  $1.5$  in order to approximate the observed background in the A band wings. Figures 12-20 show comparisons between observed and calculated spectra for selected occultation scans. (The synthetic spectra in these figures have been multiplied by the Kurucz solar transmittances. Accordingly, some of the discrepancies discussed above are not apparent in these figures.)

The agreement is generally quite good, but the calculation appears to underestimate the absorption near the band center at the longest path lengths.

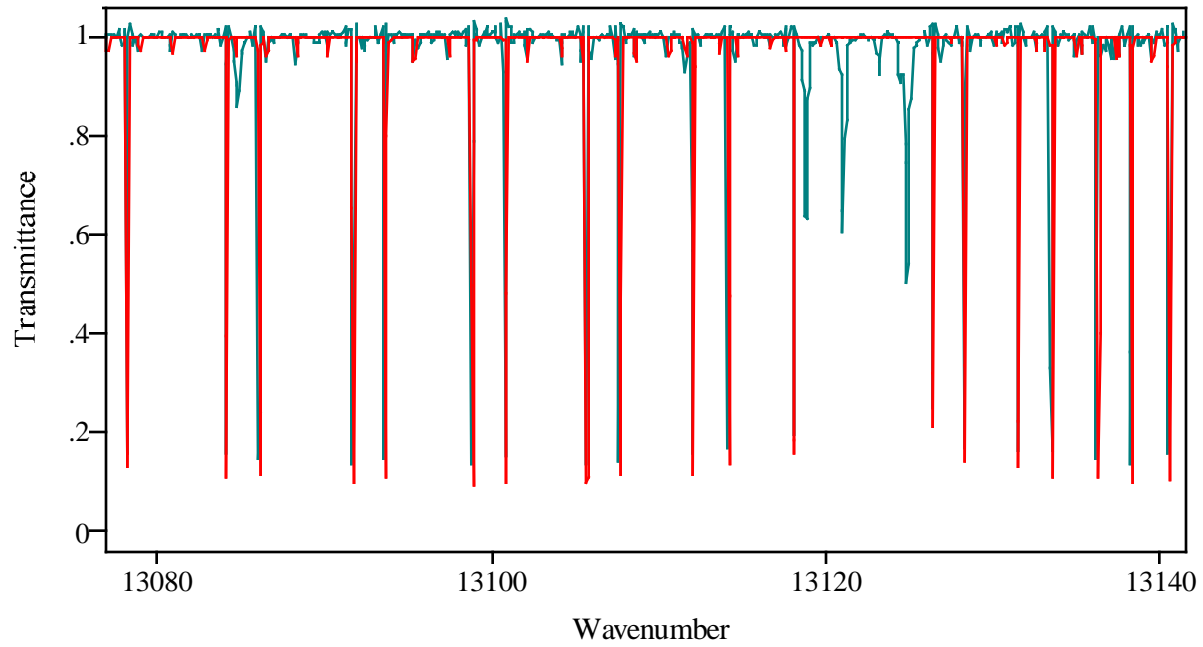


Figure 5. Averaged high sun spectrum compared to synthetic LBLTM spectrum. The lines missing from the calculation near  $13122 \text{ cm}^{-1}$  are due to absorption in the solar atmosphere.

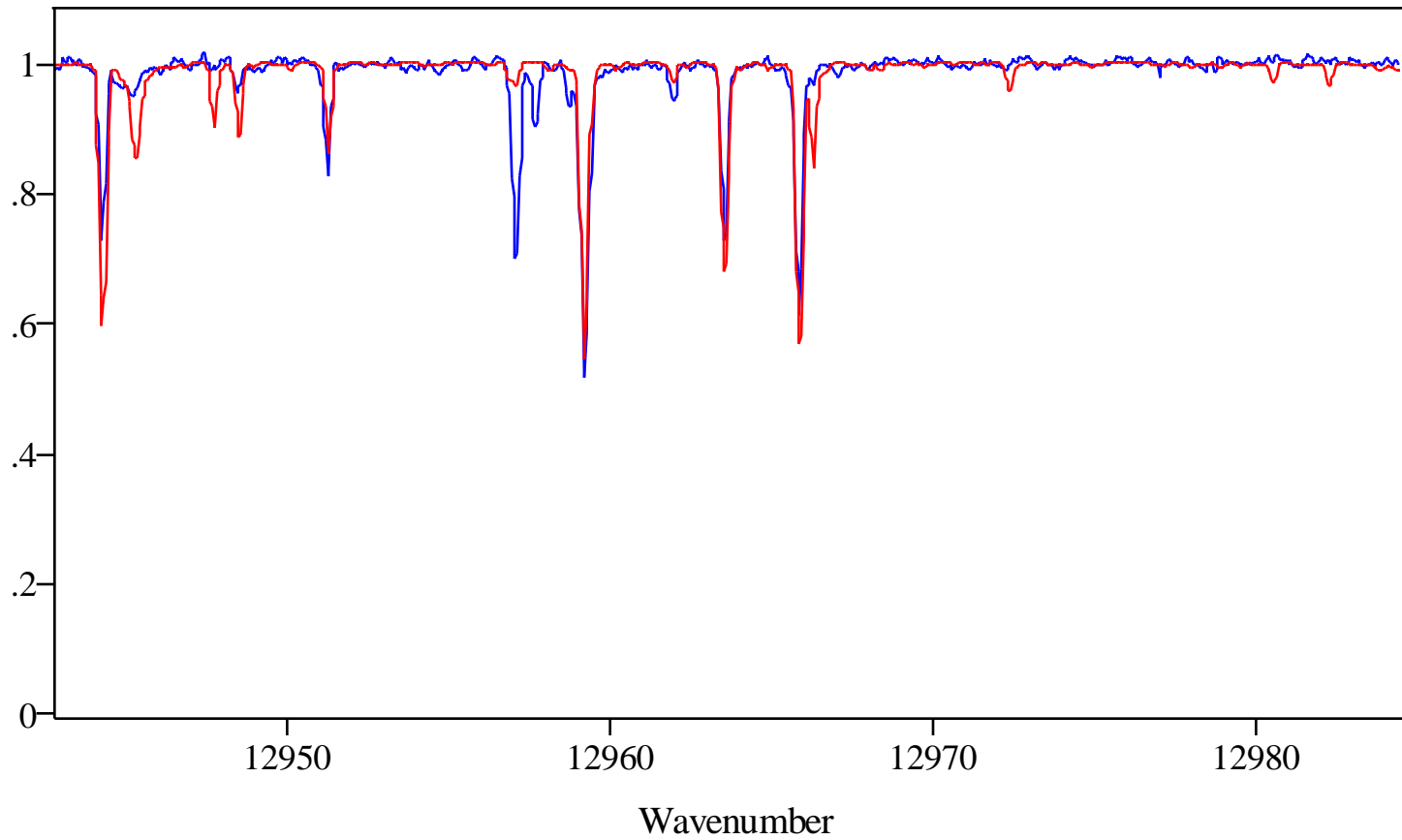


Figure 6. Comparison of averaged high sun spectrum (blue) with Kurucz solar line compilation (red). Observed solar lines near  $12958\text{ cm}^{-1}$  are missing or strongly underestimated.

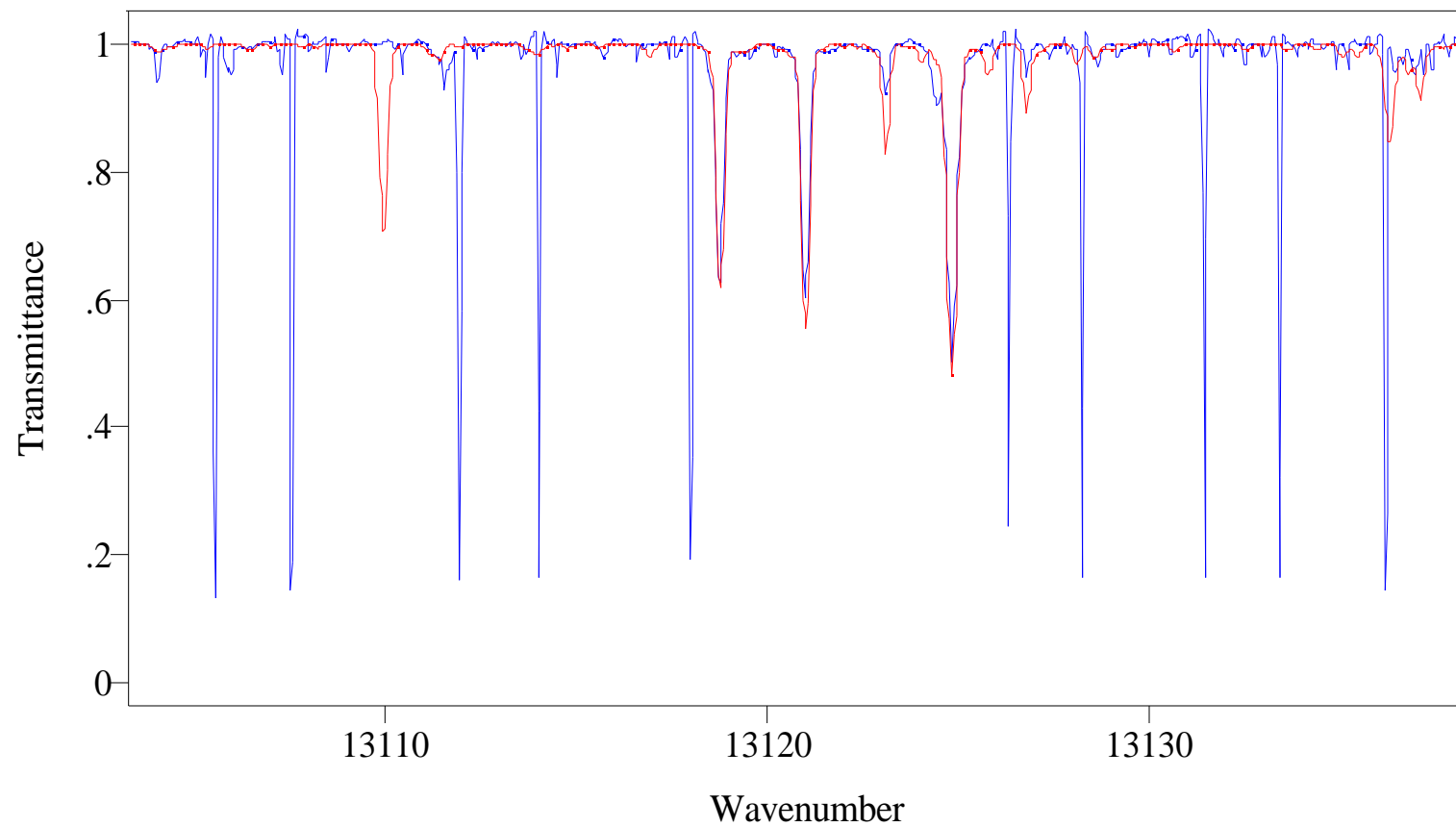


Figure 7. Comparison between averaged high sun spectrum (blue) and Kurucz solar line compilation (red). Solar lines near  $13122\text{ cm}^{-1}$  are well reproduced, but line predicted at  $13110\text{ cm}^{-1}$  does not appear in the data. (Narrow lines are due to  $\text{O}_2$ .)

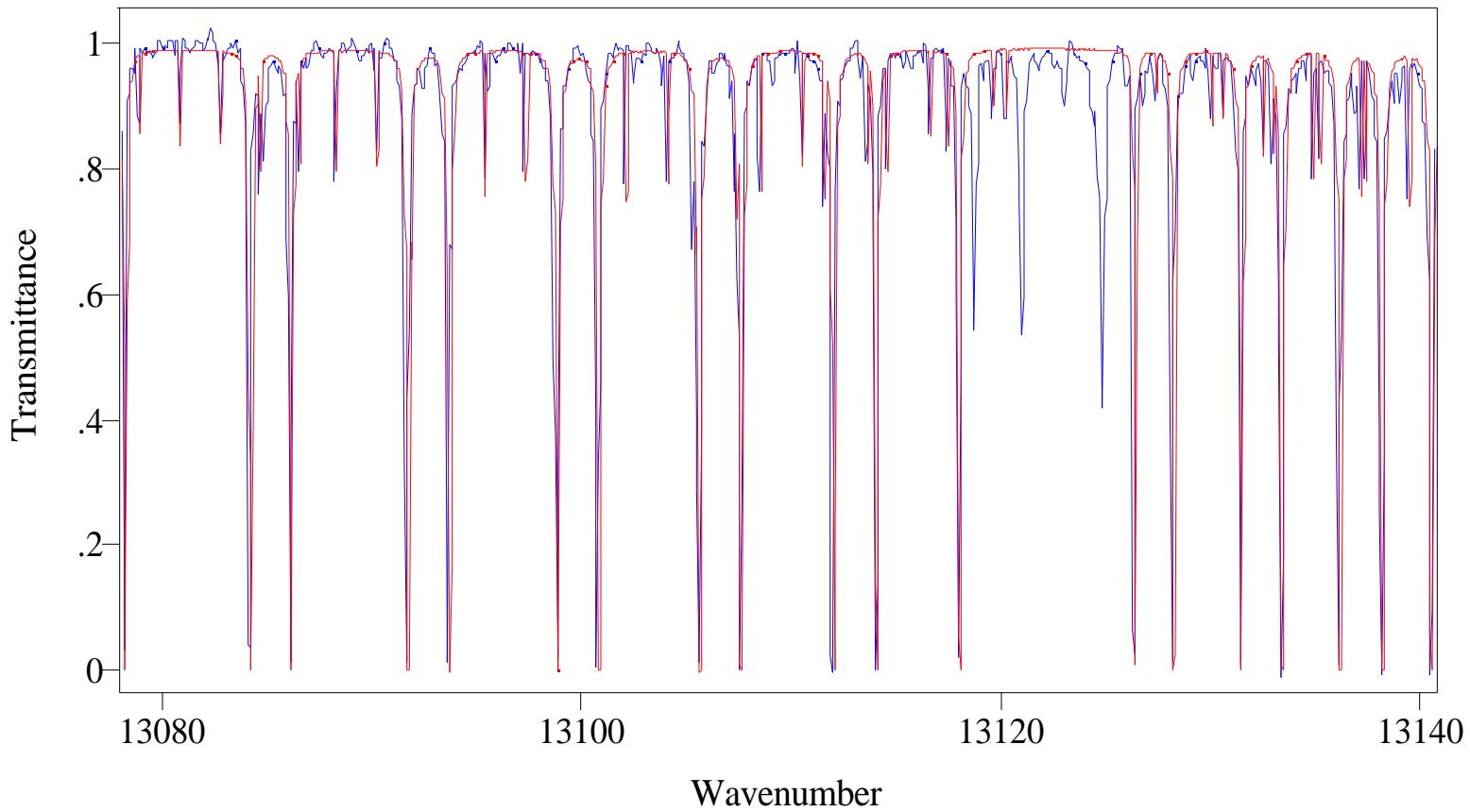


Figure 8. Comparison of ascent spectrum (blue) from 18.46 km and 68.61° with LBLRTM simulation (red).



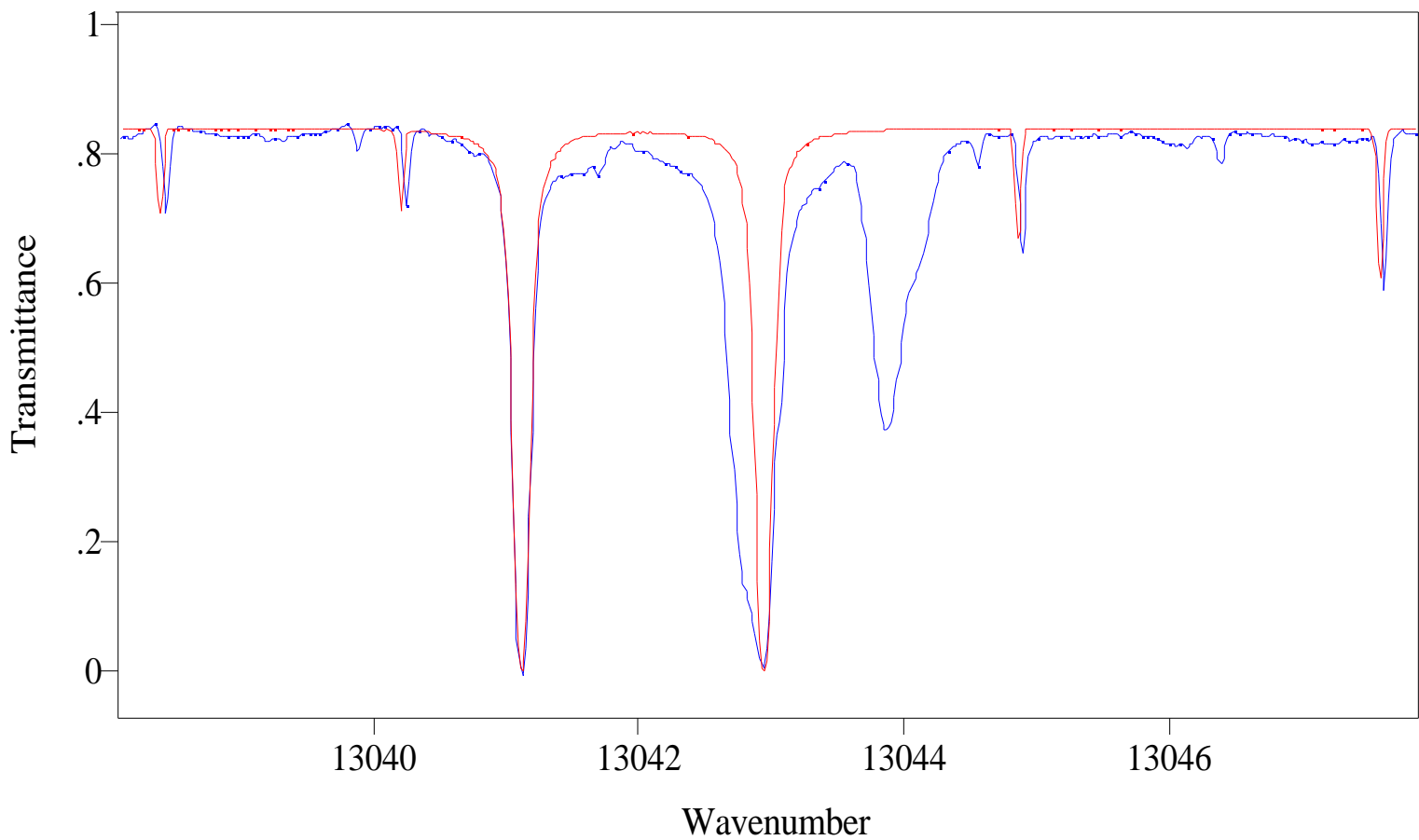


Figure 9. Comparison between observed (blue) and synthetic (red) spectra showing shifted lines of  $^{16}\text{O}^{18}\text{O}$ . The magnitude of the shift decreases toward lower  $J$  values. These missing strong lines are due to solar absorption, which was not modeled in the calculation.

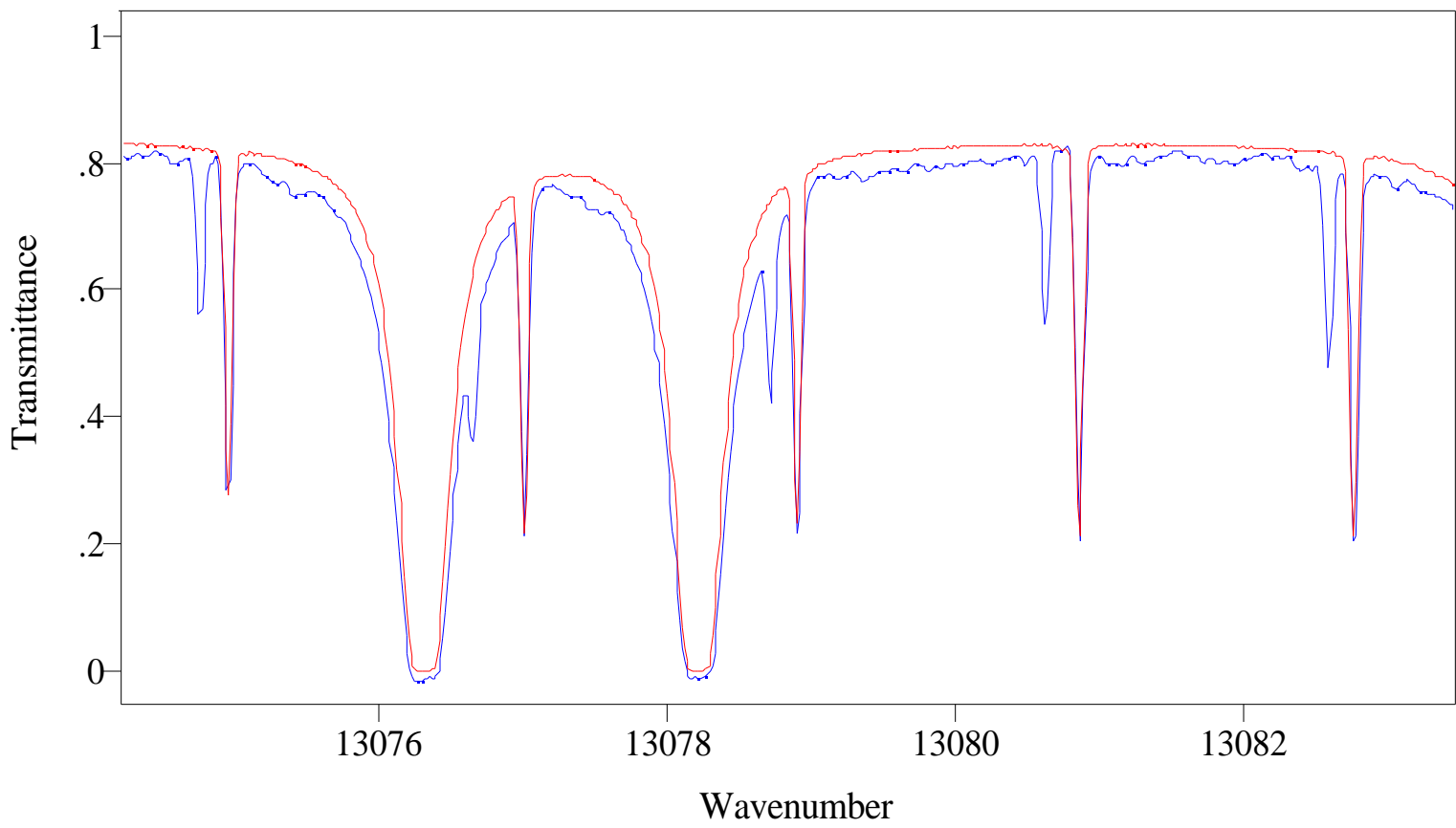


Figure 10. Observed (blue) and calculated (red) spectra showing missing  $^{16}\text{O}^{17}\text{O}$  lines. The shifted  $^{16}\text{O}^{18}\text{O}$  lines adjacent to the missing lines have come into better register as one approaches the band center.

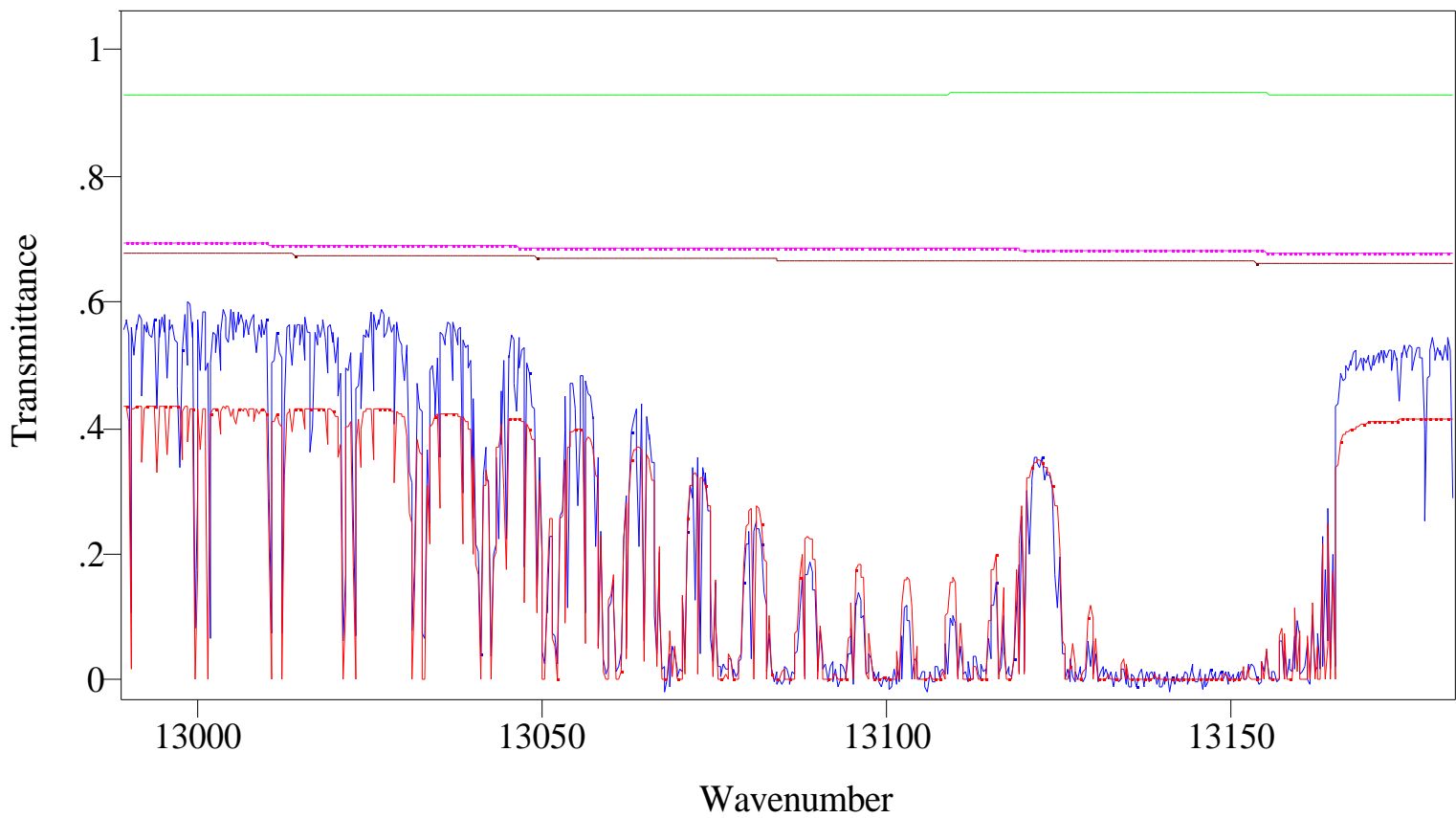


Figure 11. Comparison of observed (blue) and calculated (red) spectrum at  $94.35^\circ$ . The top three traces show the calculated contributions to the continuum due to  $O_3$ , Rayleigh, and aerosol effects, respectively. One sees that the combined computed continuum from these three sources predicts more absorption than is observed.

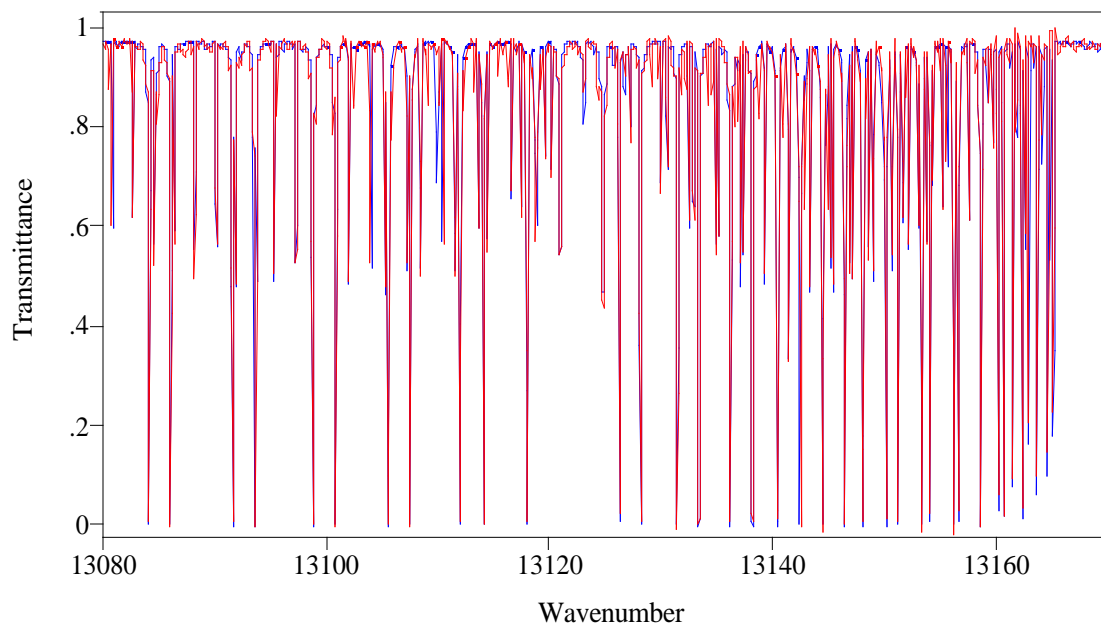
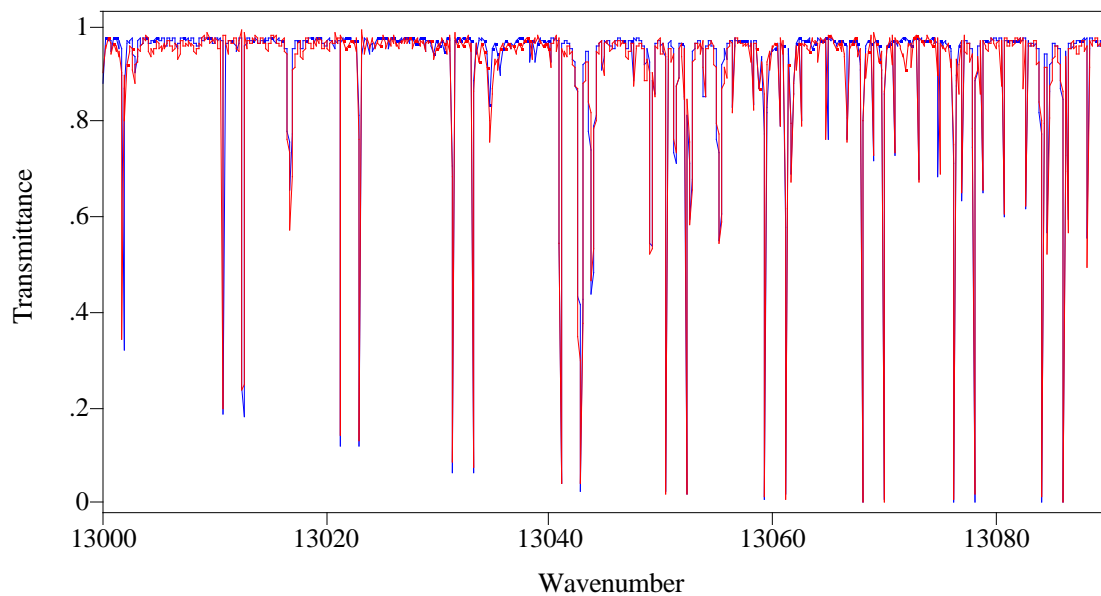


Figure 12. Observed (red) and calculated (blue) spectra at 91.24°.

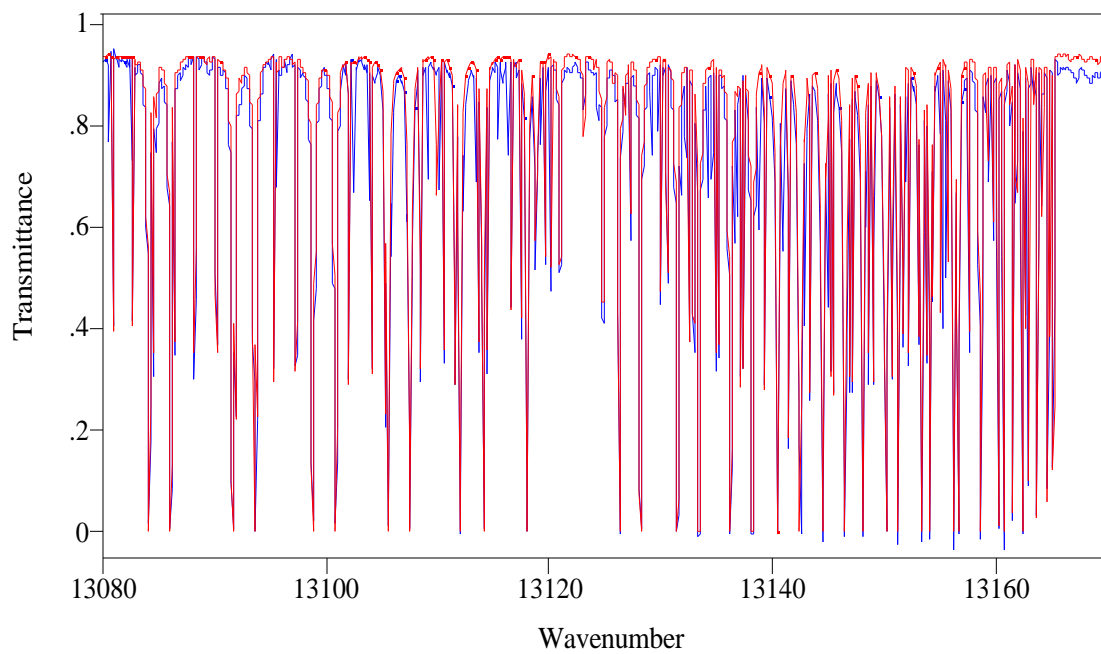
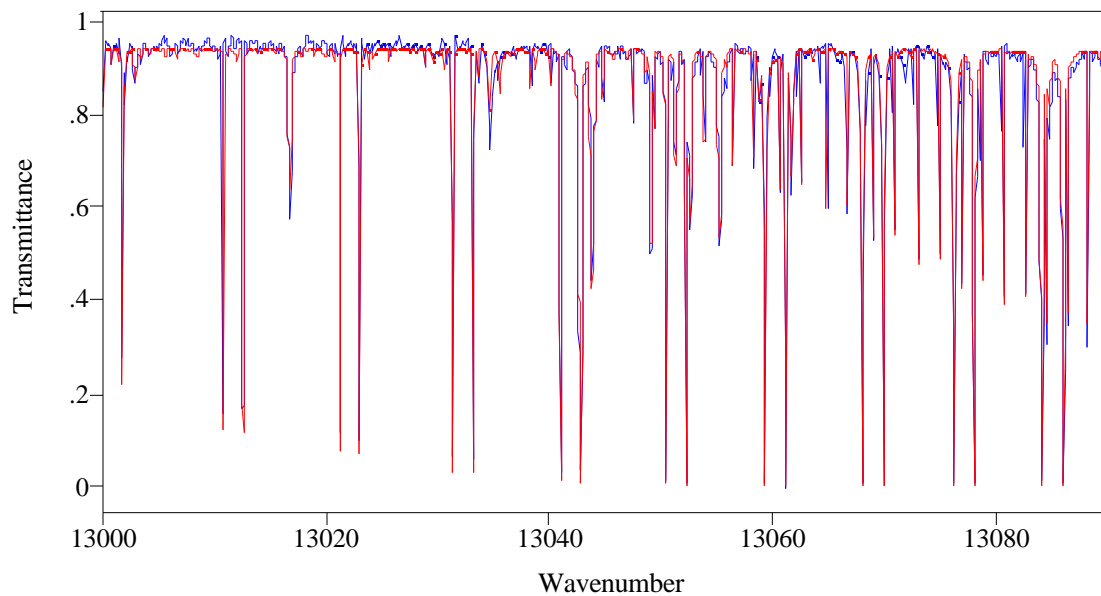


Figure 13. Observed (blue) and calculated (red) spectra at  $92.38^\circ$ .

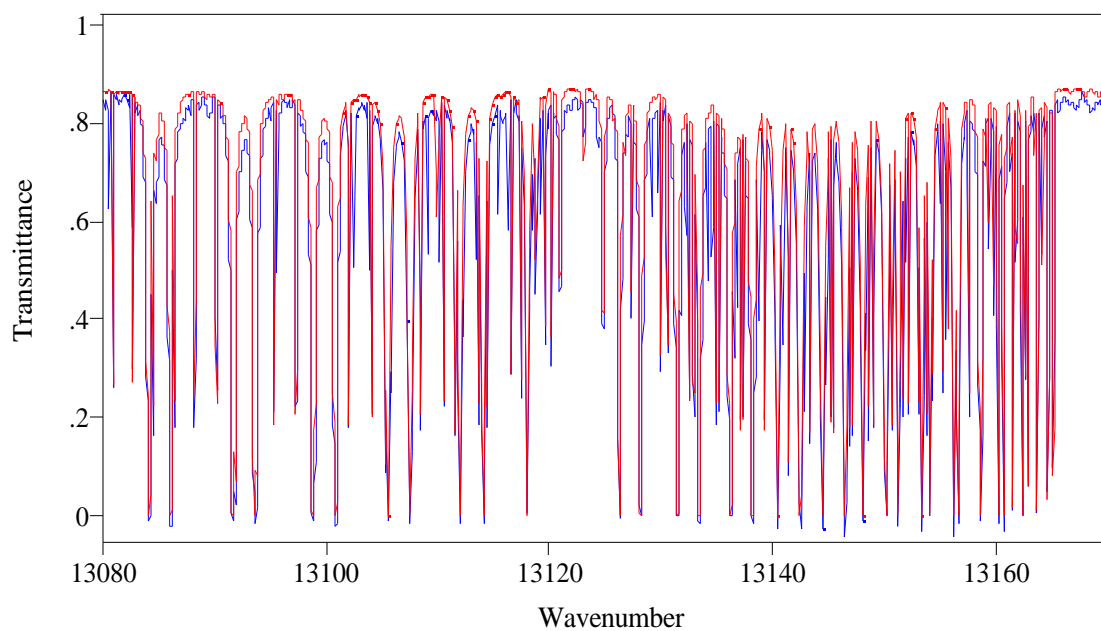
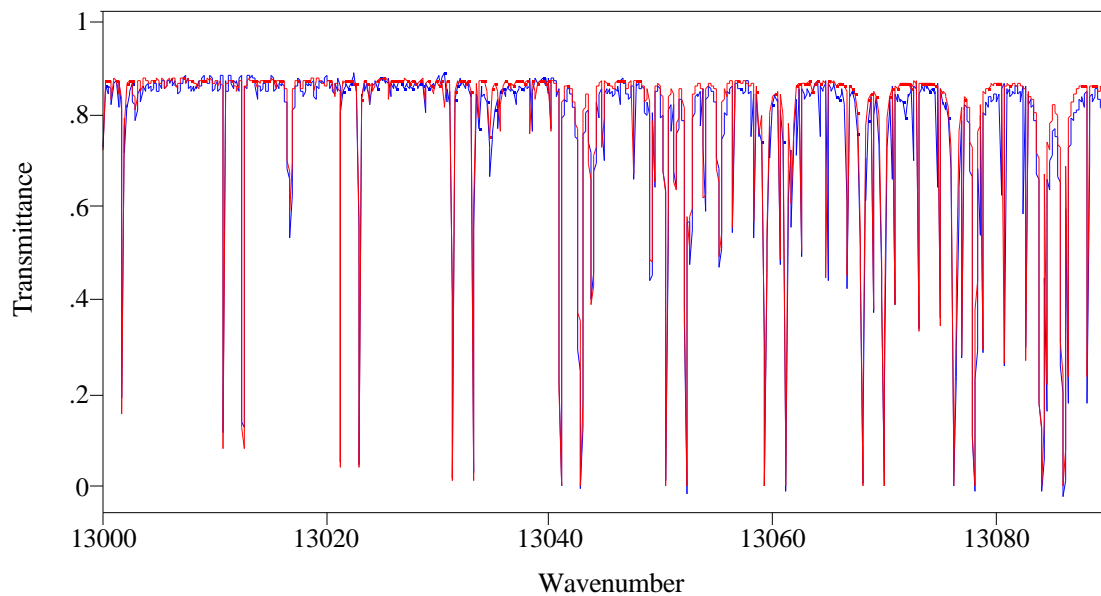


Figure 14. Observed (blue) and calculated (red) spectra at  $92.95^\circ$ .

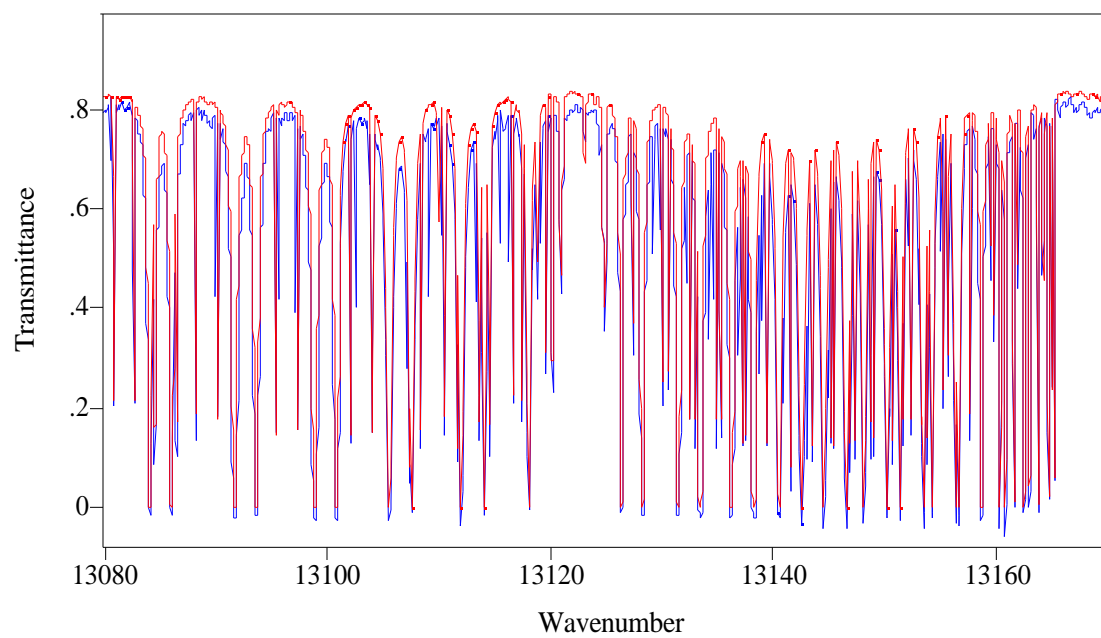
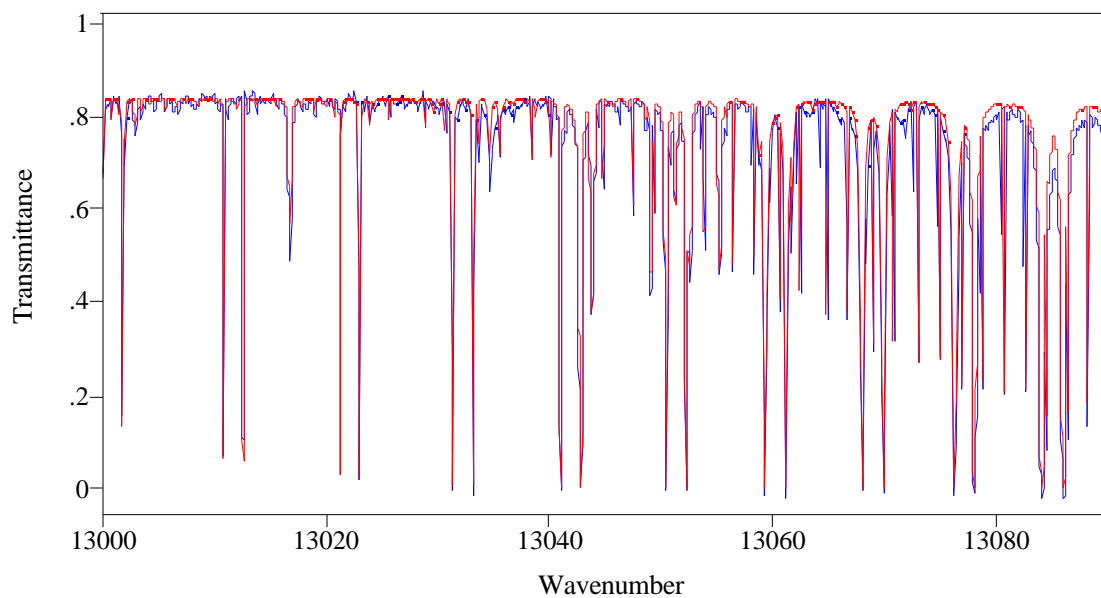


Figure 15. Observed (blue) and calculated (red) spectra at  $93.23^\circ$ .

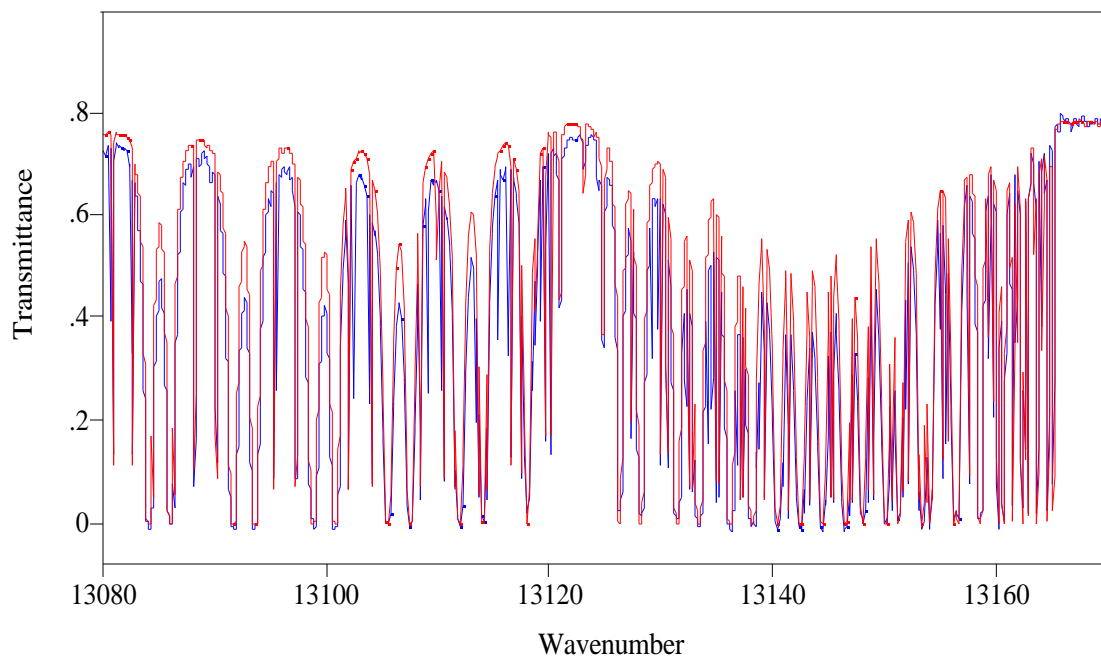
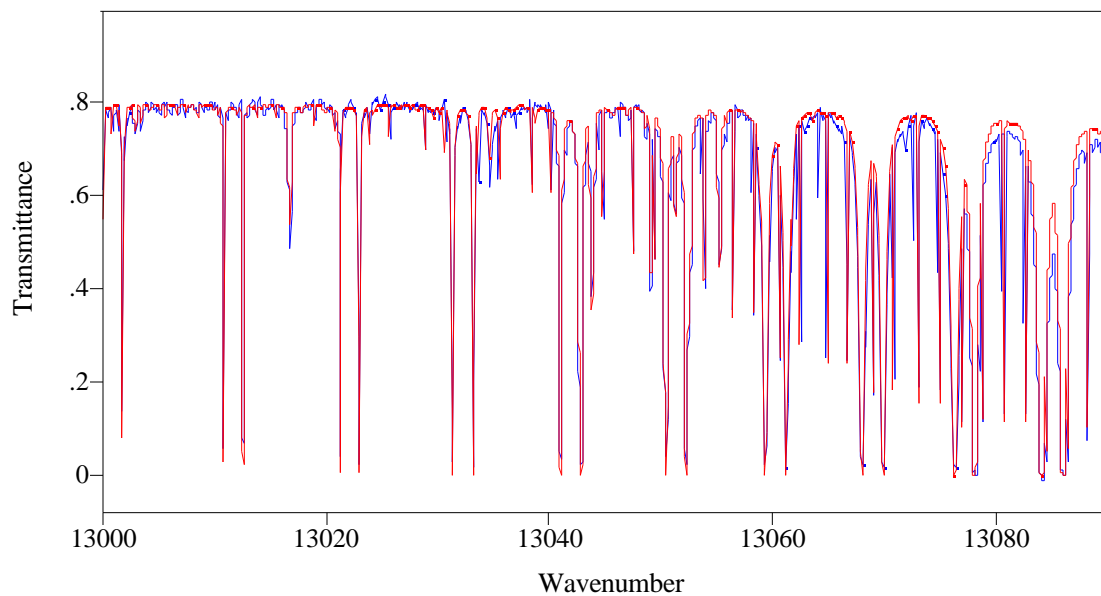


Figure 16. Observed (blue) and calculated (red) spectra at  $93.80^\circ$ .

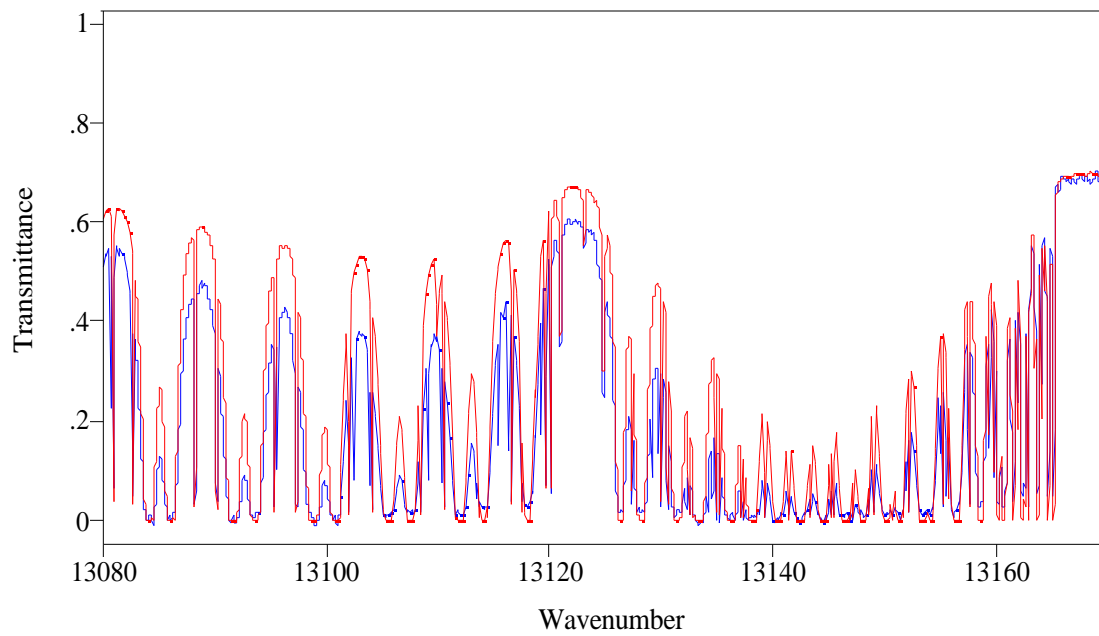
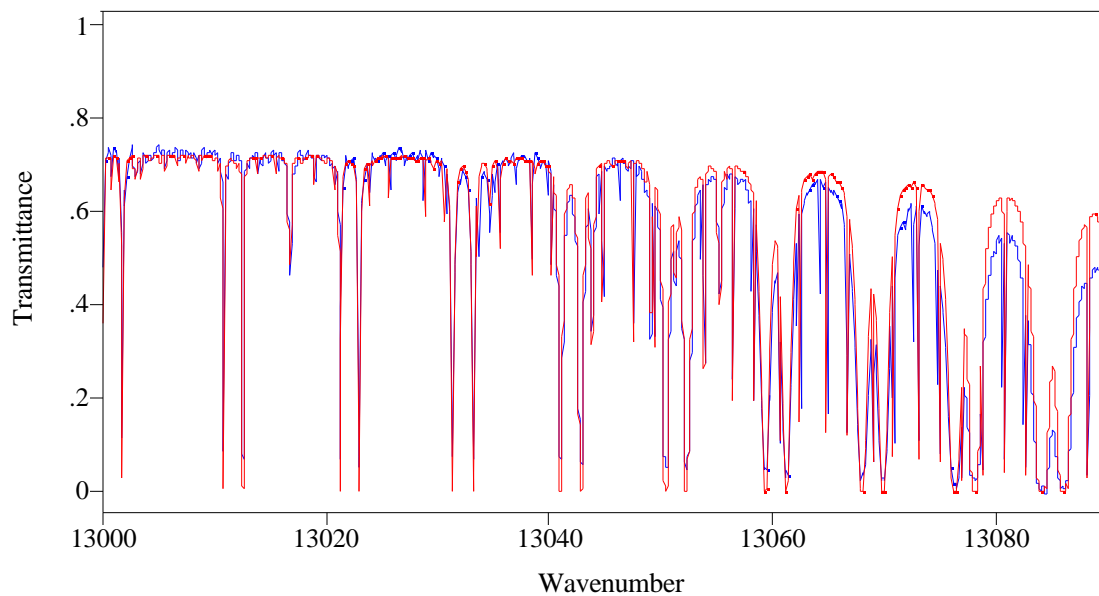


Figure 17 Observed (blue) and calculated (red) spectra at  $94.35^\circ$ .

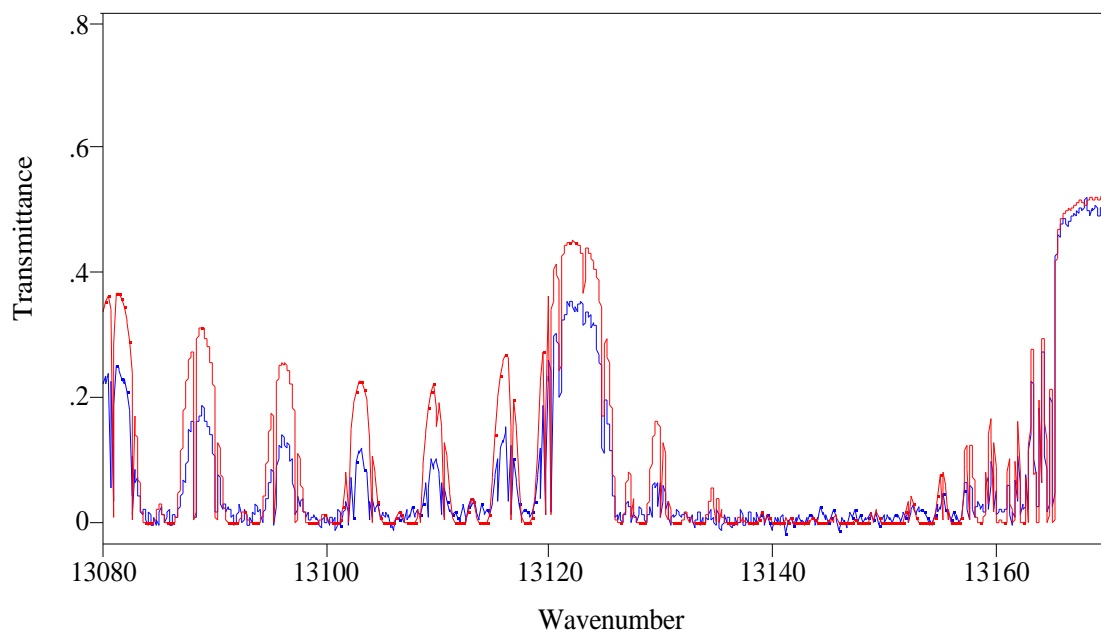
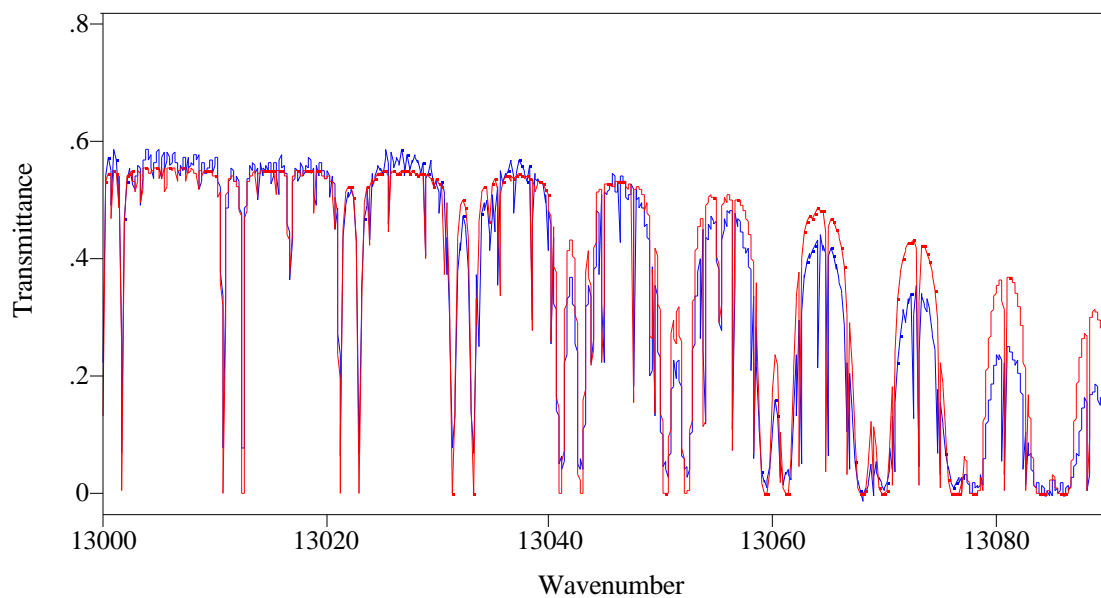


Figure 18. Observed (blue) and calculated (red) spectra at  $94.85^\circ$ .

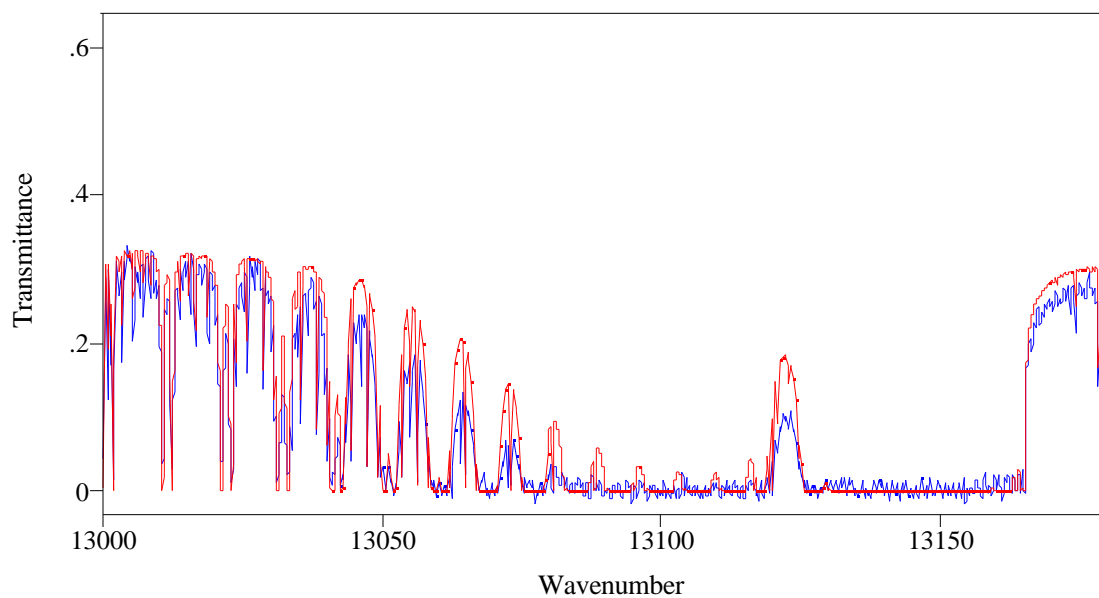


Figure 19. Observed (blue) and calculated (red) spectra at  $95.41^\circ$ .

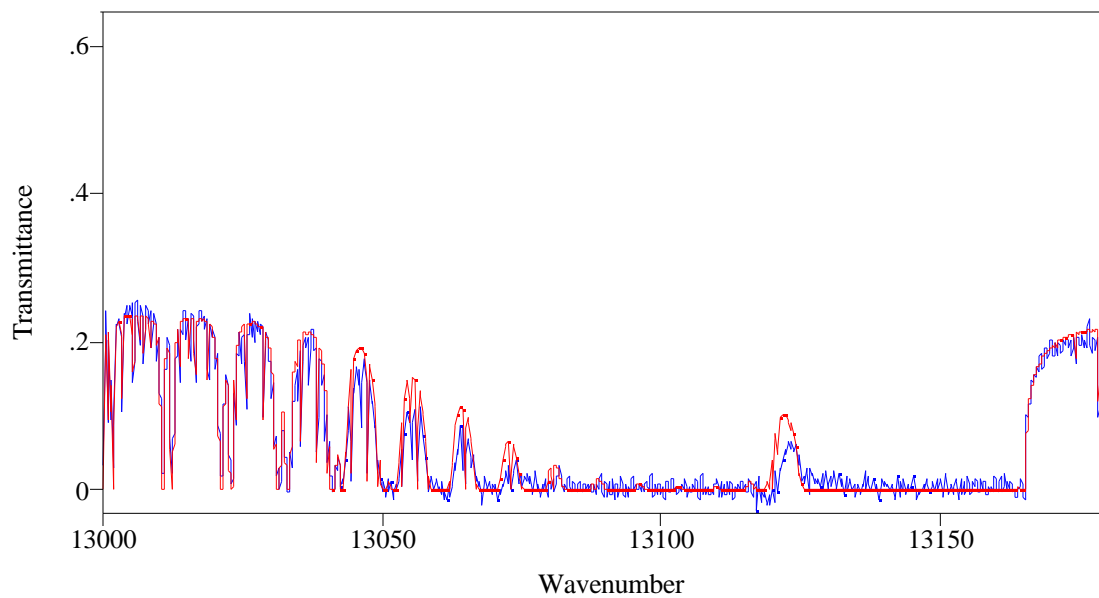


Figure 20. Observed (blue) and calculated (red) spectra at  $95.69^\circ$ .

## CONCLUSION

In this work, we have measured atmospheric absorption in the oxygen A band region from a high altitude balloon platform viewing the sun through optical paths exceeding 30 air masses. It appears that the very strong continuum absorption in this region can be accounted for by the known absorptions due to the O<sub>3</sub> Chappuis band, and a combination of Rayleigh and aerosol effects, although it will not in general be possible to distinguish between these. The O<sub>2</sub> line parameters appear to accurately characterize the oxygen absorption for air masses less than ~10, but there may still be some difficulties modeling the center of the A band region over very long paths. The modeling was complicated by inadequate line parameters for O<sub>2</sub> isotopes, missing or incorrect lines in the solar emission model, and uncertainties in aerosol effects.

## REFERENCES

Brown, L.R., and C. Plymate, Experimental line parameters of the oxygen A band at 760 nm, *J. Mol. Spectrosc.*, 199, 166-179, 2000.

Clough, S.A., M.J. Iacono, and J.-L. Moncet, Line-by-line calculations of atmospheric fluxes and cooling rates: Application to water vapor, *J. Geophys. Res.*, 97, 15,761-15,785, 1992.

Rothman, L.S., et al., The HITRAN molecular spectroscopic database and HAWKS (HITRAN Atmospheric WorkStation): 1996 edition, *J. Quant. Spectrosc. and Radiat. Transfer*, 60, 665-710, 1998.

Foreman, Michael L., W. Howard Steel, and George A. Vanasse, Correction of asymmetric interferograms obtained in Fourier spectroscopy, *J. Opt. Soc. Am.*, 56, 59-63, 1966.

Kurucz, R.L., Synthetic infrared spectra, in *Infrared Solar Physics, IAU Symp. 154*, edited by D.M. Rabin and J.T. Jefferies, Kluwer Academic Press, Norwell, MA, 1992.